

ESTIMATION OF THE TRUE LYAPUNOV SPECTRUM FOR INSTABILITY PREDICTION OF A SIMPLE NUMERICAL MODEL OF A BRAKE SYSTEM

Sebastian Oberst*, Joseph C.S. Lai

Acoustics & Vibration Unit, School of Engineering and IT, UNSW Canberra, Canberra, Australia
s.oberst@adfa.edu.au, j.lai@adfa.edu.au

Keywords: Brake Squeal, Lyapunov spectrum, Stability, Pad modes, Statistics.

Abstract. *The estimation of squeal propensity of a brake system from the prediction of unstable vibration modes using the linear complex eigenvalue analysis method has its fair share of successes and failures. While predicting complex eigenvalues in the frequency domain is almost standard practice for the automotive industry, time domain methods and the estimation of the Lyapunov spectrum have not received much attention in brake squeal analysis. The estimation of the true Lyapunov exponents to discriminate against spurious ones is still a challenge. The objective of this study is to investigate the use of statistical estimates and their robustness with respect to parameter variation based on an estimation of the Eckmann-Ruelle matrices and their Lyapunov exponents. As a benchmark, classical chaotic systems such as the Henon map are used. Results of the statistical estimators indicate that true Lyapunov exponents scatter less and have smaller variance, giving the narrowest confidence intervals. This method is applied to obtain the Lyapunov exponents from the vibration and sound pressure time traces of a simplified brake system in the form of a pad-on-plate model. The Lyapunov spectrum estimates indicate with high confidence that the plate, destabilised by the in-plane sliding direction, produces squeal. The method presented here enables a new cost-efficient method of instability estimation in conjunction with conventional FE methods.*

1 INTRODUCTION

As described in a number of review articles [1, 2, 3, 4], brake squeal as a friction-induced phenomenon may be caused by instability mechanisms of physical (eg stick slip), geometrical (e.g. sprag slip, impact) or dynamical (mode coupling, stick-slip-separation waves) origins. Despite many experimental [5], analytical minimal models [6] and numerical studies on brake squeal [7], since late 1990s, the numerical complex eigenvalue analysis (CEA) [8] has been the standard industry practice to assess brake squeal propensity at the design stage of a new brake system. However, the CEA may over or under-predict the number of unstable vibration modes [2, 9, 7]. This is due to (1) not every established limit cycle will squeal [10]; (2) contact and friction laws used are often overly simplified [11] and (3) linear analysis technique are mostly applied but brake squeal is basically a nonlinear process [12] with a possible existence of marginally stable or chaotic solutions [13]. Hence there is now a growing interest in applying nonlinear techniques to the study of brake squeal [3, 9, 14, 7]. For the predictability of nonlinear (natural) systems the maximum LYAPUNOV exponent (logarithm of Jacobian's eigenvalue [15]) is of utmost interest as it is related to the loss of long term predictability (diverging exponential separation of the trajectory). However, sometimes the spectrum of finite-time (local in the following) Lyapunov exponents would be of interest as it relates dynamic measures to static (geometrical) properties (Kaplan-Yorke conjecture), even allows viscous time-invariant damping of nonlinear systems to be estimated and could give insights into the system's stability without the necessity of model reduction (e.g. for marginally stable or chaotic solutions) [16]. For the Lyapunov spectrum, conventionally the 'Jacobian' approach is used to fit linearly the time evolution of neighbouring states' difference vectors as quasi-Jacobians [15, 17] from which the local Lyapunov exponents can be extracted [18]. However, spurious LYAPUNOV exponents result from 'over-embedding', a necessary process even when working with computationally generated time series [19]. The alternative is computationally challenging by estimating the true Jacobian in avoiding spurious exponents by fitting the attractors tangent space e.g. via principal component analysis and nontrivial projection procedure [17].

As the invariant calculation over attractor reconstruction is an estimation process, confidence intervals for Lyapunov exponents could be an useful to determine spurious Lyapunov exponents. A statistical framework based on moving block-bootstrapping has been proposed by Gencay [20] for testing chaotic dynamics via Lyapunov exponents. However, it has been argued by Ziehmann et al. [18] that bootstrapping replicates from the products of *randomly ordered Jacobians* do not give a valid tangent map (non-commutativity of matrices).

The aim of this study is to explore the use of the statistical analysis in estimating Lyapunov exponents first for the Henon map to gain some insight and then for a simple brake model in the form of a pad-on-plate [7, 21] using a methodology similar to Gencay [20] (c.f. [22]). Distributions of Lyapunov exponents are calculated using bootstrapping for different time series lengths. Bootstrapped segments of a given length are randomly selected from the original time series and the linear propagator's Jacobians [18] is calculated without randomising the elements in each segment to give a distribution of Lyapunov exponents. The key assumption for the proposed method is that the influence of noise is similar for spurious Lyapunov exponents. By contaminating the time series with a small amount of noise and examining the effect of noise on a large number of Lyapunov exponent estimates using a beta-binomial model, spurious Lyapunov exponents may be identified. Bayesian confidence intervals (credible intervals as highest density regions (HDR)) are calculated for the probability p that one Lyapunov exponent is not spurious. The stability of the pad-on-plate model over varying friction coefficients is interpreted in the

light of the dissipated energy spectrum and the process of estimating Lyapunov exponents.

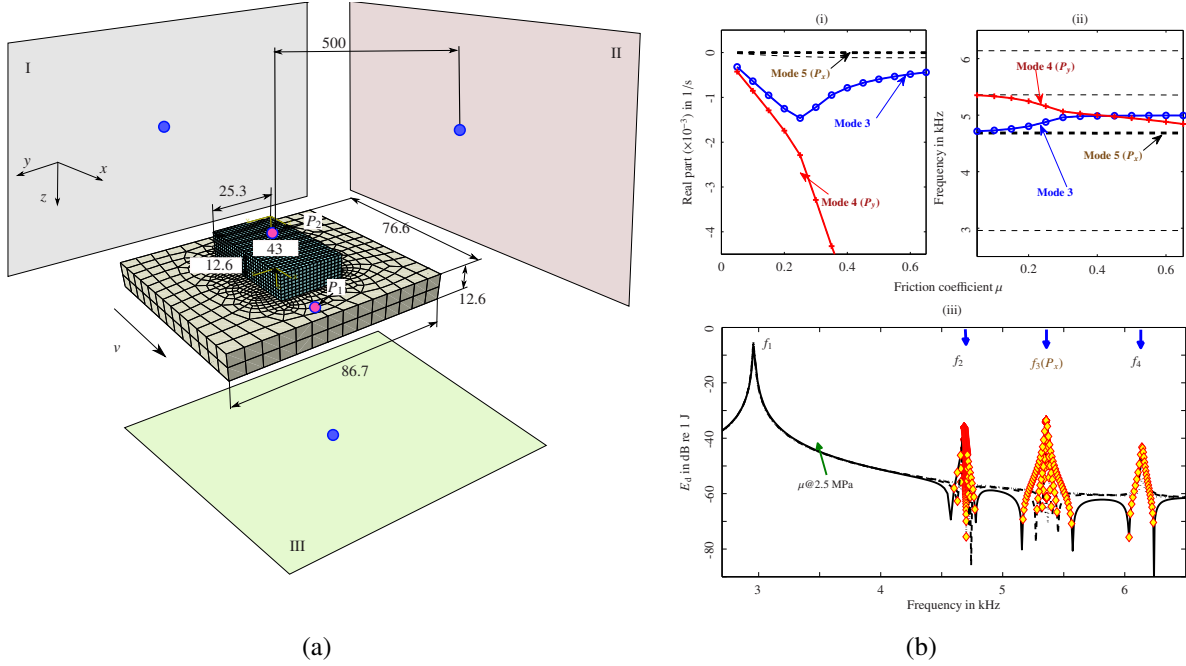


Figure 1: Pad-on-plate system [7], (a) structural mesh and schematically depicted field point mesh (panels); all dimensions in mm; (b) Real part (i) and imaginary part (ii) of a complex eigenvalue analysis (ABAQUS 6.8-4); pressure of 2.5 MPa; no instability is predicted as all real parts remain negative; (iii) spectrum of dissipated energy for $\mu = 0.05, 0.25, 0.45$ and 0.65 ; diamond markers indicate negative dissipated energy.

2 MODELS

Two models were considered: (1) the Henon map [17] $H = (x_{i+1}, y_{i+1}) = (g(x_i, y_i), h(x_i, y_i)) = (a - x_i^2 + by_i, x_i)$ with parameter settings $a = 1.4$ and $b = 0.3$ (200,000 samples), and (2) a numerical finite element pad-on-plate model (Figure 1 (a) length time series 28,000 samples, sampling frequency 14 kHz c.f.[7]) with observation functions $s(x, y; wn) = x + 0.5y + wn\delta$ (Henon map) and $s(x; wn) = x + wn x$, wn - white noise (2% output power re 1 W), are generated [17].

A pad-on-plate model [4, 7, 21] simulated using ABAQUS 6.8-4 via static nonlinear pre-stress analysis, linear modal analysis, quasi-nonlinear complex eigenvalue analysis and direct, steady-state perturbation analysis (DSA) [23]. A constant contact pressure (2.5 MPa) to the back of the pad and a constant friction coefficient (μ : 0.05, 0.25, 0.45 and 0.65) are applied. The stiffness matrix is asymmetric due to friction and a complex structural stiffness proportional damping of 4% is applied in the DSA step. The structural forced response analysis is based on a perturbation step which accounts for weak nonlinearities migrated through other steps [23, 7]. The boundary element method for calculating the acoustic response from the structural forced response is a linear analysis and only accounts for one-way coupling of the structure to the fluid. Nonlinear analysis of the time series obtained by inverse Fourier transforming the forced structural vibration and acoustic response is conducted using the TISEAN package [15].

Figure 1(a) shows results of the complex eigenvalue analysis: (i) the real parts are all negative, indicating stability; (ii) while frequency changes with friction coefficients by up to 700 Hz for mode 3 and mode 4 (dominated by either the plate or the pad motion in the y -direction).

Figure 1(b) depicts the dissipated energy spectrum for a range of friction coefficients. While the dissipated energy at the resonance frequency f_1 is always positive, the dissipated energy at resonances f_2 to f_4 (associated with the dominant pad motion in the x -direction and out-of-plane plate motion [7]) is negative (f_3 the most), indicating the potential for the system to be unstable. As no static instability (buckling) was found and at a friction coefficient of 0.0 the dissipated energy is not negative, the instability does not originate from previous static pre-stress steps.

3 METHODOLOGY

The embedding dimension is calculated using two different methods. The first method calculates a correlation dimension estimate D_2 over the logarithm of the slope of the correlation sum (discretised correlation integral; D_2 identifies e.g. fractality over different scales using an increasing ϵ -neighbourhood and embedding dimensions (here $m = 120$) [15].

The D_2 calculations have an ϵ -neighbourhood interval which is bounded by the dominating effect of noise (and the effect of having not enough neighbours in the ϵ neighbourhood; both interval endpoints are characterised by a sudden increase of the dimension estimate. This interval allows to identify the scaling region of the D_2 estimate.

Taking the interval distributions of dimension estimates over different dimensions are exponentially weighted and a 99% confidence interval (CI) of the median D_2 can be obtained. Whitney's embedding theorem states that for the embedding dimension, $m > 2 \times D_f$ (D_f , fractal dimension) has to be satisfied; here we define $m_1 = \lceil 2 \times D_2 \rceil$ the first embedding, which serves as a lower bound for a suitable embedding dimension.

The second method uses the first minimum of the mutual information to calculate a proper delay τ [13]. Then, the fast nearest neighbour algorithm [15] is applied over a sampling segment of the time series, and calculated 100 times. This embedding dimension estimate is referred to as $m_2 = \lceil m \rceil$ which gives an upper bound for the embedding dimension m^* so that $m_1 \leq m^* \leq m_2$.

From the time series, segments of random lengths are randomly chosen and for each segment, the Lyapunov spectrum is calculated. For the distribution of Lyapunov exponents $L_i, i = 1 \dots m^*$ a dispersion measure, conventionally understood as a 95% confidence interval (CI) for the median is calculated $\|I_j\|$, with $\|\cdot\|$ being the Euclidean distance, $I_j = [-\mathcal{X}_j, +\mathcal{X}_j] = x_{med} \pm 1.57 \frac{Q_{75} - Q_{25}}{\sqrt{N}}$ (Q_{75} 75th percentile, Q_{25} 25th percentile, x_{med} distribution median, for the j th iteration). The 95% confidence interval is seen in a Bayesian sense and distributions of widths of I_j s for each L_i are formed by moving a window of a predefined size over all the samples. Finally the differences in the median for different window sizes are compared for each iteration. Then, for each estimated median L_i and j , a *success* is recorded if the confidence intervals of the medians sizes do not overlap with any of the other CI. The probability of a true Lyapunov exponent is calculated from the number of successes using a beta-binomial model [24] together with the 95% credible intervals as the highest density regions (HDR) [24].

Applying this method to a white noise signal (100,000 samples, $m^* = 5$, power of 2 dB re 1 W) gives at least 2 pairs of overlapping confidence intervals for every measuring window size (1000 to 3000 samples in steps of 40), indicating no significant differences in distributions of the distance measure $\|I_j\|$. However, testing the hypothesis that L_i is a true Lyapunov exponent using the beta-binomial model and the statistics of successes and failures gives for L_5 5/50 successes in the interval 30,000 – 70,000 with a probability of the median $p = 9.47\%$ with a 95% HDR=[0.034, 0.185]. This means we are 95% sure the success rate of having 5 successes out of 50 has a probability of about 9.5%. The other Lyapunov exponents all have zero successes with $p = 0.01339 \in HDR_{95\%} = [0, 0.058]$.

4 RESULTS

Henon map For the Henon map (0% noise), the correlation dimension and embedding dimension are calculated ($\tau = 1$) as $D_2 = 1.2849 \pm 0.2326 \in \text{CI}_{99} = [1.2139, 1.3559]$ which gives and $m_1 = 2$ and $m = 5 \pm 0.3505 \in \text{CI}_{99} = [2.0404, 2.2396]$, such that m_2 and $m^* = 3$; however, an over-embedding of $m^* = 5$ is chosen to compare results with [17].

By contaminating the time series with noise ($\delta = 0.10$), the estimate of the correlation dimension D_2 and the embedding dimension m change to $D_2 = 0.9869 \pm 0.6668 \in \text{CI}_{99} = [0.6378, 1.3361]$ and $m = 6.36 \pm 0.88 \in \text{CI}_{99} = [6.1, 6.6]$; so $m^* = 7$ with $m_1 = 1 \leq m^* \leq m_2$ would be an appropriate embedding. While the true dimension ($D_2 = 1.25827$ [19]) is contained within the confidence interval of the correlation dimension estimate, the change in the embedding dimension m reflects the effect of noise on the reconstruction of the attractor in phase space.

Figures 2 (a) to (d) depict the results of the Lyapunov spectrum for the Henon map using $m = 5, m = 7$, for $\delta = 0.0$ in (a) and (c) and $\delta = 0.01$ in (b) and (d). The first row gives the estimation of Lyapunov exponents over different time series lengths with their median plotted as black lines; the two true Lyapunov exponents $L_1 = L_{\max} = +0.42$ and $L_2 = L_{\min} = -1.62$ indicated by arrows. The Lyapunov exponents in (a) and (b) scatter very little around their mean value; the noisy data in (c) and (d) have visibly more outliers. An 'avoided crossing of Lyapunov exponents' [17] is visible in Figure 2 (a), where the value of true maximum Lyapunov exponent (0.41) is approximated for time series length below 80,000 Samples L_2 . However, as the neighbourhood size (30) remains unchanged, this non-crossing does not seem to be due to the gradual domination of high-order nonlinear expansion terms [17] but rather to the 'non-convergence' as a combination of the time series not being long enough. Over-embedding (Figure 2(b)) causes this 'convergence' process to be *delayed*; e.g. the L_1 does not predict the real Lyapunov exponent by using a time series of only 200,000 iterations. ?

The noise introduced in Figure 2(c) and (d) pushes the first Lyapunov exponent onto their 'converged' values, especially L_{\max} but also the spurious exponents L_2 to L_4, L_7 which is in the direction of contracting dynamics, does not converge using a time series of about 200,000 samples. The use of $m = 7$ (Figure 2(d)) slightly degrades the convergence of L_i , visible for small sample sizes.

The second row in Figure 2 exemplifies the width of the 95% confidence interval I_j for all L_i over samples after bootstrapping over a intervals length of 1000 samples and minimising the effect on curvature for non-converged values using a linear global correction for the trend. L_i s of time series below 15,000 samples seem unreliable based on comparisons with widths of the 95% confidence intervals for using segments of more samples. For the noise free cases (a) and (b), the 95% confidence interval is narrower for segments of 15,000 – 85,000 samples probably owing to a constant neighbourhood size parameter of 30 [15]; for a larger number of cycles more spurious data points are recorded. Over-embedding also degrades the estimation process; especially L_6 shows larger deviations which is even more the case for noise contaminated calculations (d).

The third row in Figure 2 depicts box plots I_j based on Lyapunov exponents calculations based on data depicted in the second row (measuring window 1,000 samples, 10% overlap). For the box plots non-overlapping notches between boxes show significant differences in width at the 95% level. For the box plots in column (a) L_i between 15000 – 80000 (before the crossing), for (b)-(d) the whole interval after segments length of 15000 samples are considered. In (a) the I_j of the second Lyapunov exponent is significantly different from the other I_j . Taking L_i s of segment lengths of 80000 – 200000 samples, L_1 has a significantly different median interval width.

However, for the noise free cases (a) and (b) the true negative Lyapunov exponent cannot

be elaborated by I_j . If noise is added I_j belonging to L_5 (c) and L_7 (d) become in median the largest. The I_j s medians of the L_{\min} and L_{\max} are significantly different but not those of the spurious exponents (in (c) L_2 and (d) L_3 or L_2-L_6). L_4 in (c) shows also a significantly different median of I_j but only for this measuring window width of 1000.

For the noisy cases (c) and (d) the measuring window is varied from 1000 to 3000 samples and increasing its size by 40 segment lengths each time (i.e. 1000, 1040, 1080, ... , 3000). For all L_i a statistic of the number of events (successes and failures) is build up based on non-overlapping notches of I_j which represent successes. The beta-binomial model gives for $L_1 = L_{\max}$ ($m = 5$ & $m = 7$) and $L_7 = L_{\min}$ a 100% success rate and a median estimated probability of $p = 0.9865$ being true Lyapunov exponents in a 95% HDR interval of $[0.9413, 1.0]$. For L_5 (Figure 2(c) $m = 5$) the estimated probability is $p = 0.9666$ in a 95% HDR interval of $[0.91, 1.0]$. As the correlation dimension indicates with high confidence that only two Lyapunov exponents are expected, the other Lyapunov exponents (L_2 , L_3 and L_4/L_6) are very likely spurious hence no probabilities are calculated here.

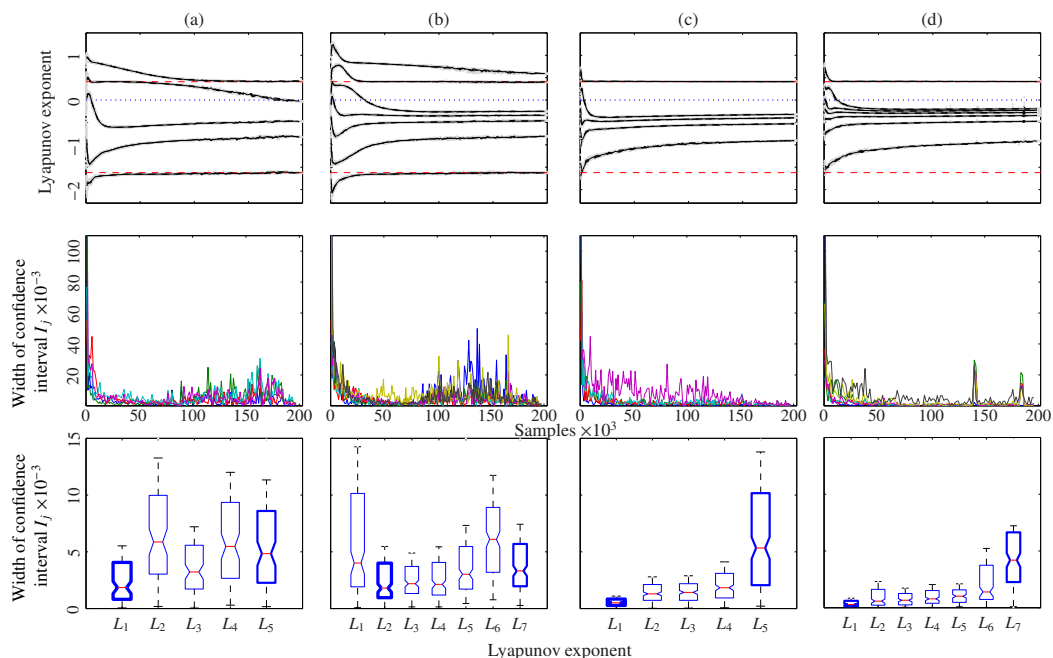


Figure 2: Estimation of Lyapunov spectrum (solid line median, top row), I_j (width of confidence intervals) of L_i corrected by global trend (middle row) and box plots I_j (bottom row) for the Henon map with $\delta = 0$ (a), $m = 5$, (b) $m = 7$, and $\delta = 0.01$ (c) $m = 5$, and (d) $m = 7$.

In case of the Henon map noise improves the prediction of the largest Lyapunov exponent (smoothing) and degrades the prediction of the smallest Lyapunov exponent (c.f. [25]). Increasing the noise level from zero to 0.1, 1, 10% and 20% (not depicted), the median curve of the Lyapunov exponent in the contracting direction (L_5 or L_7 for $m = 5$ and $m = 7$ respectively) is shifted to higher values; embedding in higher dimensions shows that spurious Lyapunov exponents are contained between the largest and the smallest Lyapunov exponents [17].

In summary, (1) not every Lyapunov exponent converges to the true value; a spurious Lyapunov exponent may predict the correct numerical value. The time series has to be as long as necessary with an embedding dimension as small as possible to calculate the Lyapunov spectrum. (2) Spurious L_i s converge quickly to false estimates as soon as noise is introduced; comparing different dimension estimates and with different noise levels will also allow potentially spurious

Lyapunov exponents to be identified [19]. Spurious exponents which cluster around zero, may render predictions of true and near zero L_i s difficult. Zero Lyapunov exponents have to be estimated with complementary analysis such as dimension estimates or qualitatively by plotting the reconstructed attractor in phase space. (3) The true L_i s are influenced by noise differently, indicated by a significantly different median I_j .

Numerical Pad-on-Plate model The time series of the pad motion in the x -direction at P_1 , P_2 and in the centre point of the plane opposite to the pad (Figure 1(a)) is analysed (noise $\delta = 0$ and $\delta = 0.01$, $\mu = 0.45$) using the same procedure as for the Henon map (Figure 3 (a) and (b)). Only segment lengths over 10,000 were taken into account.

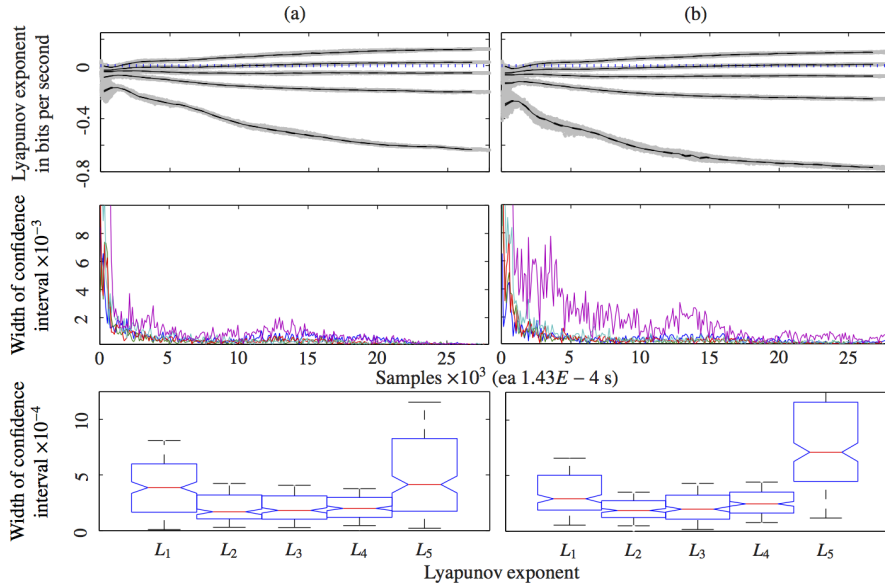


Figure 3: Pad-on-plate model: Estimation of Lyapunov spectrum (median) and calculated exponents (grey dots), I_j for all L_i corrected by the global trend and box plots of I_j (bottom row) using $m = 5$ (a) $\delta = 0.0$, (b) and $\delta = 0.01$]

The addition of noise sharpens the estimation procedure: while three Lyapunov exponents do not show significant differences in their estimated medians of the I_j , the largest and the smallest exponent have significantly different median values. Only the zero Lyapunov exponent representing a regular motion caused by the driving frequency is distinguishable from the other L_i s which cluster around zero. However, phase space plots show that between the most negative and the positive Lyapunov exponent lies at least one with zero as the attractor shows an underlying regular motion (c.f. Oberst and Lai [21]).

For all friction coefficient the correlation dimension increases by 1 and the pad is not getting more positive Lyapunov exponents. The phase space dynamics indicate, that the motion must lie on a torus (delay embedding [15]). Applying the beta-binomial model to the estimation of the median width of the 95% confidence interval I_j by using a moving window (overlap 10%) with changing size (i.e. going by 50 samples each time, from 100 to 1050) gives for L_1 the probability $p = 0.9614 \in HDR_{95\%} = [0.8364, 1]$ and for L_5 the probability $p = 0.6169 \in HDR_{95\%} = [0.3982, 0.8327]$ to be true Lyapunov exponent estimates. All other Lyapunov exponents have 0/16 successes and their probability of being true Lyapunov exponents is estimated to be $p = 0.0.03931 \in HDR_{95\%} = [0, 0.1631]$

Table 1: D_2 is the correlation dimension estimate with 99% confidence bounds; \mathcal{L}_{spec} are the LYAPUNOV exponent median estimates; the dynamic regimes (Dyn.): +, 0 and – stand for average local divergence (instability), regular circular motion (periodicity) and contraction (stability), [16, 19]; S stands for signal, v_i is the velocity in direction i (x, y, z), p is the sound pressure.

	S	D_2	$\mu_{0.05}$ \mathcal{L}_{spec}	Dyn.	D_2	$\mu_{0.25}$ \mathcal{L}_{spec}	Dyn.	D_2	$\mu_{0.45}$ \mathcal{L}_{spec}	Dyn.	D_2	$\mu_{0.65}$ \mathcal{L}_{spec}	Dyn.
Plate	v_x	$2.15_{1.2}^{3.0}$	0.03 -0.01 -0.50	0 0 –	$2.5_{2.0}^{3.0}$	0.03 0.00 -0.49	0 0 –	$2.3_{0.7}^{4.0}$	0.10 0.02 -0.39	+	$2.2_{0.9}^{3.9}$	0.07 0.00 -0.45	+
	v_y	$2.1_{1.3}^{2.8}$	0.00 -0.01 -0.25	0 0 –	$2.1_{0.8}^{3.4}$	0.01 -0.02 -0.41	0 0 –	$2.1_{0.8}^{3.4}$	0.01 -0.02 -0.42	0 0 –	$3.0_{2.1}^{3.8}$	0.06 0.00 -0.04 -0.58	+
	v_z	$2.0_{1.6}^{2.5}$	0.03 -0.02 -0.47	0 0 –	$2.1_{1.0}^{3.1}$	0.00 -0.02 -0.36	0 0 –	$3.2_{2.0}^{4.4}$	0.10 0.03 -0.03 -0.54	+	$3.0_{1.6}^{4.4}$	0.08 0.01 -0.05 -0.53	+
Pad	v_x	$2.7_{1.8}^{3.5}$	0.15 0.00 -0.66	+	$2.1_{0.8}^{3.8}$	0.06 -0.02 -0.64	+	$2.3_{0.8}^{3.7}$	0.12 0.03 -0.63	+	$2.3_{1.0}^{3.6}$	0.08 0.00 0.63	+
	v_y	$2.1_{1.7}^{2.5}$	0.01 0.00 -0.17	0 0 –	$2.2_{1.8}^{2.5}$	0.00 -0.01 -0.17	0 0 –	$2.0_{1.8}^{2.1}$	0.00 -0.01 -0.17	0 0 –	$2.2_{1.8}^{2.5}$	0.01 -0.01 -0.06	0 0 –
	v_z	$1.1_{1.0}^{1.1}$	0.02 -0.47	0 –	$1.1_{1.0}^{1.1}$	0.00 -0.40	0 –	$1.9_{1.5}^{2.4}$	0.01 -0.01 -0.61	0 0 –	$2.1_{1.6}^{2.5}$	0.00 -0.05 -0.29	0 0 –
Fluid	p_z	$1.1_{1.0}^{1.2}$	0.00 -0.40	0 –	$1.2_{1.0}^{1.3}$	0.00 -0.48	0 –	$2.3_{1.8}^{3.2}$	0.01 -0.01 -0.60	0 0 –	$2.0_{1.1}^{2.9}$	0.03 -0.02 -0.30	0 0 –

Results of estimating the Correlation dimension and the Lyapunov spectrum of the vibration response of the plate, the pad (in x , y and z directions) and the fluids response in z -direction perpendicular to top of the pad (0.5 m distance) are displayed the Table 1. As the Lyapunov exponents for the motion of the pad in the y -direction are mostly zero or negative, the pad motion in the y direction does not get unstable, that of the plate only at $\mu = 0.65$. The motion of the pad in x -direction is always unstable even for small friction coefficients.

Based on the correlation dimension and the Lyapunov exponents, the dynamic regimes for the plate and the pad in the three directions are given in column ‘Dyn.’ (Table 1). A + indicates (short time) prediction loss and can be interpreted as chaotic; 0 indicates regular motion, hence a double zero is regular motion on a 2-torus (c.f. [12]); a – indicates volume contraction (dissipation). While for low friction coefficients the plates motion in the x -direction is confined to a quasi-periodic torus, with increasing μ it destabilises and seems to become chaotic. For all friction coefficients, the pad’s motion in the x -direction remains chaotic and that in the y -direction stays quasi-periodic; the motion in the z -direction undergoes a bifurcation to quasi-periodicity for $\mu = 0.45$. Here, the plate’s z -dynamics destabilises too but remain on a torus. This is similar to Oberst [7] where the chaotic pad motion triggers the instability of an annular disc (c.f. [16]). The fluids dynamics also changes from periodic ($\mu = 0.05, 0.25$) to quasi-periodic ($\mu = 0.45, 0.65$). The estimation of the dynamics based on the Lyapunov spectrum compares nicely with the correlation dimension estimates. A 2-torus has a topological dimension of 2 which is also the case when 2 zero Lyapunov exponents are found. Once the system is destabilised for $\mu = 0.45$ and $\mu = 0.65$, the dimension estimate of the plate’s dynamics in the z -direction increases from 2 to 3. The pad’s correlation dimension is fractal (2.3). The Kaplan-Yorke dimension $D_{KY} = k + \frac{\sum_i^k L_i^+}{|L_{k+1}^-|}$ also shows the same dimensions as the correlation dimension estimate which supports the estimation of the Lyapunov exponents and is on average only $2 \pm 5\%$ different from the correlation dimension estimate [16].

5 DISCUSSIONS AND CONCLUSIONS

Even if the dynamics of a system is deterministic, it is impossible to determine all Lyapunov exponents directly using the Jacobian approach because of the inherent uncertainty in the

estimated reconstructed phase space. In this study, it has been shown that uncertainty, however, could be a tool for determining spurious Lyapunov exponents by contaminating the time series with a small amount of noise and bootstrapping subsequent Lyapunov exponent calculations. By moving a measuring window with different sizes over the width of a 95% confidence interval I_j based on calculations of Lyapunov spectra credible intervals for the maximum (L_{\max}) and the minimum Lyapunov exponent (L_{\min}) can be estimated by applying a beta-binomial model of successes and failures with respect to the median width of the I_j s. For true Lyapunov exponents, the median I_j is significantly different from that of spurious Lyapunov exponents and gives high probabilities to be true exponents. Spurious Lyapunov exponents showed the strongest relative shift towards a clustering region (which was for the Henon map slightly below zero) compared to a noise free time series. The noise in the environment of the deterministic trajectory of the Henon map has less influence in the direction of expansion and a large influence in the direction of contraction [25]. Similarly Yang et al. assume that covariant Lyapunov vectors associated with spurious exponents have a higher probability to stay outside the true tangent space [17].

The procedure applied to the Henon map has been applied to the time series of a pad-on-plate model with friction and indicates that the pad at $\mu = 0.45$ has three Lyapunov exponents, one of which is positive with a fractal dimension of 2.3. Using only one single window of $74ms$ (hence no credible interval estimation) to calculate the median I_j for the other directions and friction coefficients allows to give insights into the dynamics of the pad-on-plate system and identifies the pad being the trigger for the instability. An increase in μ is associated in an increase of the L_{\max} for plate motion and sound pressure.

ACKNOWLEDGEMENTS

This research was undertaken with the assistance of resources provided at the National Computational Infrastructure National Facility through the National Computational Merit Allocation Scheme supported by the Australian Government. The first author acknowledges receipt of a University College Postgraduate Research Scholarship (UCPRS) and a Research Publication Fellowship for preparing this manuscript.

REFERENCES

- [1] N.M. Kinkaid, O.M. O'Reilly, and P. Papadopoulos. Automotive disc brake squeal. *Journal of Sound and Vibration*, 267:105–166, 2003.
- [2] H. Ouyang, W. Nack, Y. Yuan, and F. Chen. Numerical analysis of automotive disc brake squeal: a review. *International Journal of Vehicle Noise and Vibration*, 1:207–231, 2005.
- [3] N. Hoffmann and L. Gaul. Friction induced vibrations of brakes: Research fields and activities. *SAE Technical Paper Series*, 2008-01-2579:1–8, 2008.
- [4] F. Chen. Automotive disk brake squeal: an overview. *Int. J. Vehicle Design*, 51(1/2):39–72, 2009.
- [5] O. Giannini, A. Akay, and F. Massi. Experimental analysis of brake squeal noise on a laboratory brake setup. *Journal of Sound and Vibration*, 292:1–20, 2006.
- [6] U. von Wagner, D. Hochlenert, and P. Hagedorn. Minimal models for disk brake squeal. *Journal of Sound and Vibration*, 302:527–539, 2007.

- [7] S. Oberst. *Analysis of Brake Squeal Noise*. PhD thesis, University of New South Wales, University College, School of Engineering and Information Technology, March 2011.
- [8] S. Oberst and J.C.S. Lai. A critical review on brake squeal and its treatment in practice. In *Internoise 2008, Shanghai, 2008*.
- [9] D. Hochlenert. Nonlinear stability analysis of a disk brake model. *Nonlinear Dynamics*, 58:63 – 73, 2009.
- [10] K. Shin, J.-E. Oh, and M.J. Brennan. Nonlinear analysis of friction induced vibrations of a two-degree of freedom model for disc brake squeal. *JSME International Journal Series C*, 45:426–432, 2002.
- [11] T. Butlin and J. Woodhouse. Sensitivity of friction-induced vibration in idealised systems. *Journal of Sound and Vibration*, 319:182–198, 2009.
- [12] S. Oberst and J.C.S. Lai. Statistical analysis of brake squeal noise. *Journal of Sound and Vibration*, 330:2978 – 2994, 2011.
- [13] S. Oberst and J.C.S. Lai. Chaos in brake squeal noise. *Journal of Sound and Vibration*, 330:955 – 975, 2011.
- [14] J.-J. Sinou. Transient non-linear dynamic analysis of automotive disc brake squeal - on the need to consider both stability and non-linear analysis. *Mechanics Research Communications*, 37:96 – 105, 2010.
- [15] H. Kantz and T. Schreiber. *Nonlinear time series analysis*. Cambridge University Press, 2004.
- [16] J. M. Nichols, M. D. Todd, M. Seaver, S. T. Trickey, L. M. Pecora, and L. Moniz. Controlling system dimension: A class of real systems that obey the KaplanYorke conjecture. *Proceedings of the National Academy of Sciences*, 100(26):15299–15303, 2003.
- [17] Hong-liu Yang, Günter Radons, and Holger Kantz. Covariant lyapunov vectors from reconstructed dynamics: The geometry behind true and spurious lyapunov exponents. *Phys. Rev. Lett.*, 109:244101, Dec 2012.
- [18] C. Ziehmann, L.A. Smith, and J. Kurths. The bootstrap and lyapunov exponents in deterministic chaos. *Physica D*, 126:49–59, 1999.
- [19] J.C. Sprott. *Chaos and time-series analysis*. Oxford University Press, 2006.
- [20] R. Gencay. A statistical framework for testing chaotic dynamics via lyapunov exponents. *Physica D*, 89:261 – 266, 1996.
- [21] S. Oberst and J.C.S. Lai. The role of pad modes and nonlinearity in instantaneous mode squeal. In *21th International Congress on Acoustics (ICA 2013) in Montreal, 2 - 7 June, Canada, 2013*.
- [22] D. Lai and G. Chen. Statistical analysis of lyapunov exponents from time series: A jacobian approach. *Mathl. Comput. Modelling*, 27:1–9, 1998.

- [23] S. Oberst, J.C.S. Lai, and S. Marburg. Guidelines for numerical vibration and acoustic analysis of disc brake squeal using simple models of brake systems. *Journal of Sound and Vibration*, 332(9):2284-2299, 29 April 2013 2013.
- [24] J. Albert. *Bayesian Computation with R*. Springer, Wien, New York, 2012.
- [25] V.S. Anishchenko, A. S. Kopeikin, T. E. Vadivasova, G. I. Strelkova, and J. Kurths. Influence of noise on statistical properties of nonhyperbolic attractors. *Phys. Rev. E*, 62:7886–7893, Dec 2000.